# Statistics of SINR in 3-D Environment With Correlated Log-Normal Shadowing

Xiang Liu and Jing Xu

***Abstract*— Based on the stochastic geometry theory, the analysis for the statistics of signal-to-noise-and-interference ratio (SINR) is conducted in this letter, where the links between the base stations and user equipments are impaired by correlated log-normal shadowing in 3-D environment. The closed-form expressions of the statistics of signal-to-interference ratio, signal-to-noise ratio, and SINR are presented. Then, the distribution of $\text{SINR}^{-1}$ is approximated by the log-Pearson type III distribution based on the moments of $\text{SINR}^{-1}$. Numerical results indicate that the cell coverage increases with the increase of the correlation coefficient between communication and interference links.**

***Index Terms*— Stochastic geometry, 3D, correlated shadowing.**

## I. Introduction

THE system performances including the cell coverage and cell average data rate of cellular communication networks can be calculated based on the distribution of signal-to-noise-and-interference ratios (SINRs), which are jointly determined by the network geometry and channel model. Traditionally, the locations of base stations (BSs) are planned, and cellular networks are modeled as the hexagonal grid model [1]. However, analytic results for SINR are difficult to be obtained based on the hexagonal grid model [2]. Further, due to various irregularities for the actual deployment of BSs, the locations of BSs will not exactly follow the hexagonal grid model but in a more random case [2], [3].

By modelling the BSs' locations as the stochastic point process, the stochastic geometry theory has shown its tractability in dealing with interference [3], [4]. In [5], the BSs' locations in 2D plane are modeled as the Poisson Point Process (PPP), based on which the distribution of the distance between the interference BSs and the user equipment (UE) can be well characterized. Recent works have considered the extension of [5] to more general network geometry, which is well summarized in [3] and [4]. The analysis for the impact of the height of the BSs is conducted in [6] and [7]. For tractability of analysis, in [5]–[7], the closed-form expressions for the cell coverage and cell average data rate are obtained based on some specific channel conditions, where the communication link is impaired by the Rayleigh/Rice fading and correlations of the channel fading between the communication and interference links are ignored.

However, log-normal distribution but not Rayleigh distribution is the commonly used distribution to model the channel fading of the link connecting the BS and UE [8], [9]. Moreover, with the increase of the density of BSs, the correlation of shadowing for the links formed by the geographically proximate interference BSs and UE cannot be ignored [8], [10]. The correlated log-normal shadowing in 2D environment is considered in [11]. However, in [11], the closed-form expressions for the system performances are not available.

To the best of our knowledge, none of the existing works have derived the closed-form distribution of SINR for the PPP-based networks considering the correlated log-normal shadowing in 3D environment. In this letter, the system performance for communication networks with the homogenous PPP (HPPP) located BSs is studied. The main contributions of our work are as follows:

- The analysis for the statistics of SINR for a more practical channel model is conducted, where the shadowing for the communication and interference links in 3D environment are modeled as the correlated log-normal random variables.
- The closed-form expressions for the statistics of SIR, SNR and SINR, i.e., the moments of $\text{SIR}^{-1}$, $\text{SNR}^{-1}$ and $\text{SINR}^{-1}$ are presented, the analytical results show that $\lambda_B h_B^2$ is the underlying factor for the statistics of SIR, where $\lambda_B$ and $h_B$ represent the density and height of BSs, respectively.
- Numerical results indicate that the distribution of $\text{SINR}^{-1}$ is well approximated by the log-Pearson type III distribution. The cell coverage increases with the increase of the correlation coefficient between communication and interference links.

The letter is organized as follows. Section II briefly introduces the network geometry and channel model. The statistics of SINR are analyzed in Section III. The system performance based on the approximate distribution of SINR is given in Section IV. Numerical investigations upon the height of BSs and correlation coefficient are provided in Section V. Conclusions are drawn in Section VI.

## II. System Model

### A. Network Geometry

The locations of the BSs and UEs in the 2D horizontal plane are modeled as the two-dimensional homogeneous PPP $\Psi_B$ and $\Psi_U$ with a density of $\lambda_B$ and $\lambda_U$, respectively [5]. The antenna heights of the BSs and UEs are assumed to be $h'_B$ and $h'_U$, respectively. The height difference between the antenna of BS and UE is denoted as $h_B$, i.e., $h_B = h'_B - h'_U$.

Manuscript received May 27, 2018; accepted June 25, 2018. Date of publication July 5, 2018; date of current version September 8, 2018. This work was supported in part by the National Natural Science Foundation of China (Grant No. 61571303), in part by the Inter-Government Key Program for International Scientific and Technological Innovation Cooperation Project of China (Grant No. 2016YFE0122900), and in part by the Shanghai Municipal Natual Science Foundation (Grant No. 16ZR1435100). The associate editor coordinating the review of this letter and approving it for publication was D. Cassioli. *(Corresponding author: Jing Xu.)*

The authors are with the Science and Technology on Micro-system Laboratory, Shanghai Institute of Microsystem and Information Technology, Chinese Academy of Sciences, Shanghai 200050, China, and also with the University of Chinese Academy of Sciences, Beijing 100049, China (e-mail: xiang.liu@wico.sh; jing.xu@wico.sh).

Digital Object Identifier 10.1109/LCOMM.2018.2853104

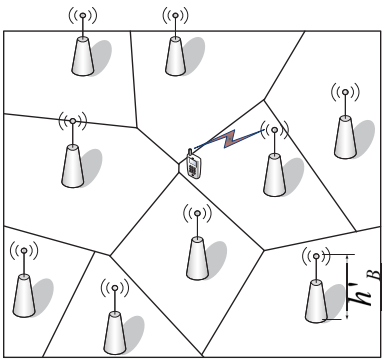


Fig. 1. Network geometry.

We make the same assumption as in [6], in which each UE is associated with its closest BS, for that the closest BS can offer a maximum expected power for the connection. As shown in Fig. 1, the locations of BSs and the UE under consideration are depicted. Without loss of generality, we assume that the antenna of the UE under consideration is located at the origin.

Spherical coordinated system is adopted to describe the locations of BSs and UE. The location of the antenna of BS$_i$ is denoted as $(\sqrt{R_i^2+h_B^2}, \Theta_i, \Phi_i)$, $R_i$ represents the 2D distance between the BS$_i$ and UE in the horizontal plane. $\Theta_i$ and $\Phi_i = \arctan\frac{h_B}{R_i}$ represent the azimuth angle and elevation angle of the link connecting the antenna of BS$_i$ and UE, respectively.

The location of the antenna of UE is $(0,0,0)$. Then the location of the antenna of the serving base station BS$_0$ is $(\sqrt{R_0^2+h_B^2}, \Theta_0, \Phi_0)$, $R_0 < R_i$, BS$_i \in \Psi_B$. According to the analysis in [5], the distribution of $R_0$ is expressed as

$$f_{R_0}(r_0) = 2\pi\lambda_B r_0 \exp\big(-\pi\lambda_B r_0^2\big), \quad r_0 \in (0,\infty). \tag{1}$$

### B. Channel Model

The received power of the UE from BS$_i \in \Psi_B$ is

$$P_{BS_i} = P_t G_B X_i S_i, \tag{2}$$

where $P_t$ and $G_B$ represent the transmit power and antenna gain of BS$_i$, respectively. $X_i$ and $S_i$ denote the distance-dependent path loss and log-normal shadowing for the link connecting the antenna of BS$_i$ and UE, respectively. $S_i$ is assumed to be independent of the distance between UE and BS$_i$ [8]. The distance-dependent path loss is expressed as

$$X_i = A(R_i^2+h_B^2)^{-\beta/2}, \tag{3}$$

where $A$ and $\beta$ represent the distance-dependent path loss at reference distance and the path loss exponent, respectively.

In [8] and [11], the channel model for the correlated log-normal shadowing is introduced, in which the shadowing of the link between the antenna of BS$_i$ and UE is modeled as

$$S_i = \exp(\xi\sigma\sqrt{1-\rho}W_i + \xi\sigma\sqrt{\rho}Z), \tag{4}$$

where $\xi = \frac{\ln 10}{10}$, $W_i$ and $Z$ are independent and identically zero-mean Gaussian random variable with unit variance, respectively, i.e., $W_i \overset{i.i.d}{\sim} \mathcal{N}(w_i;0,1)$ and $Z \sim \mathcal{N}(z;0,1)$.

## III. Statistics of SINR

The downlink SINR of the typical UE can be calculated as

$$\text{SINR} = \frac{P_{BS_0}}{\sigma_N^2 + \sum_{i,BS_i\in\Psi_B/BS_0} P_{BS_i}}, \tag{5}$$

where $\sigma_N^2$ represents the noise power of the system. Then according to the expression of SINR shown in (5), the reciprocal of SINR can be calculated as

$$\frac{1}{\text{SINR}} = \frac{\sigma_N^2 + \sum_{i,BS_i\in\Psi_B/BS_0} P_{BS_i}}{P_{BS_0}} = \frac{1}{\text{SNR}} + \frac{1}{\text{SIR}}, \tag{6}$$

where SNR and SIR represent the signal-to-noise ratio and signal-to-interference ratio, respectively,

$$\text{SNR} = \frac{P_{BS_0}}{\sigma_N^2},$$
$$\text{SIR} = \frac{P_{BS_0}}{\sum_{i,BS_i\in\Psi_B/BS_0} P_{BS_i}}.$$

### A. Analysis of SIR

In this subsection, the statistics of SIR are analyzed. According to the expression of the received power for the typical UE as shown in (2), the reciprocal of SIR is calculated as

$$\frac{1}{\text{SIR}} = \frac{\sum_{i,BS_i\in\Psi_B/BS_0}\big(R_i^2+h_B^2\big)^{-\beta/2}\exp(\xi\sigma_\rho W_i)}{\big(R_0^2+h_B^2\big)^{-\beta/2}\exp(\xi\sigma_\rho W_0)}, \tag{7}$$

where $\sigma_\rho = \sigma\sqrt{1-\rho}$. Then the moments of SIR$^{-1}$ can be obtained based on the following lemma.

*Lemma 1:* The $n$th moment of SIR$^{-1}$ can be calculated as

$$m_n\left(\frac{1}{\text{SIR}}\right) = \exp\left(\frac{n^2\xi^2\sigma_\rho^2}{2}\right)\exp\big(\pi\lambda_B h_B^2\big) \times \sum_{\bigcup_{p=1}^q I_p = I^n} \times \left[\begin{matrix} 2^q\Gamma\big(q+1,\pi\lambda_B h_B^2\big) \\ \times\prod_{p=1}^q (n_p\beta-2)^{-1}\exp\left(\frac{n_p^2\xi^2\sigma_\rho^2}{2}\right)\end{matrix}\right], \tag{8}$$

where $\Gamma(a,b) = \int_b^\infty u^{a-1}e^{-u}du$ denotes the incomplete Gamma function. The summation runs through the list of all partitions of a set $I^n = \{1,2,\ldots,n\}$ with size $n$. $I_p, p = 1,2,\ldots,q$ represent the different parts of one partition, $q$ represents the number of parts for the partition and $n_p$ is the number of the elements of the certain part $I_p$ [12].

For example, for $n = 3$, $I^n = \{1,2,3\}$, and there are 5 partitions for the set $I^n$, for the certain partition: $I_1 = \{1,2\}, I_2 = \{3\}$, then $q = 2$, and the elements in the parts $I_1$ and $I_2$ are $n_1 = 2$ and $n_2 = 1$, respectively.

*Proof:* Let

$$J = \sum_{i,BS_i\in\Psi_B/BS_0}\big(R_i^2+h_B^2\big)^{-\beta/2}\exp\big(\xi\sigma_\rho W_i\big). \tag{9}$$

Then according to [13], the $n$th cumulant of $J$ given $R_0 = r_0$ can be calculated as

$$c_n(J|R_0=r_0) = \frac{2\pi\lambda_B\big(r_0^2+h_B^2\big)^{-n\beta/2+1}}{n\beta-2}\exp\left(\frac{n^2\xi^2\sigma_\rho^2}{2}\right).$$

The $n$th moment of $J$ given $R_0 = r_0$ is

$$\mathbb{E}\left(J^n|r_0\right) = \sum_{\bigcup_{p=1}^{q} I_p = I^n} \left[ \prod_{p=1}^{q} \frac{2\pi\lambda_B \left(r_0^2 + h_B^2\right)^{-n_p\beta/2+1}}{n_p\beta - 2} \times \exp\left(\frac{n_p^2\xi^2\sigma_\rho^2}{2}\right) \right].$$

Since the $n$th moment of $\text{SIR}^{-1}$ is calculated by

$$\mathbb{E}((\text{SIR}^{-1})^n) = \int_{r_0}\int_{w_0} \left( \begin{matrix} \left(r_0^2 + h_B^2\right)^{n\beta/2} \exp(-n\xi\sigma_\rho w_0) \\ \times \mathbb{E}\left(J^n|R_0 = r_0\right) f_{R_0}(r_0) f_{W_0}(w_0) \end{matrix} \right) dw_0 dr_0,$$

where $f_{W_0}(w_0) = \mathcal{N}(w_0; 0, 1)$ represents the PDF of $W_0$,

$$\mathbb{E}((\text{SIR}^{-1})^n) = e^{n^2\xi^2\sigma_\rho^2/2} \int_0^{+\infty} \left( \begin{matrix} \sum\limits_{\cup_{p=1}^{q} I_p = I} (2\pi\lambda_B)^q \left(r_0^2 + h_B^2\right)^q \\ \times e^{-\pi\lambda_B r_0^2} 2\pi\lambda_B r_0 \prod\limits_{p=1}^{q} \frac{e^{n_p^2\xi^2\sigma_\rho^2/2}}{n_p\beta - 2} \end{matrix} \right) dr_0,$$

the $n$th moment of $\text{SIR}^{-1}$ can be calculated as shown in (8). ■

According to the result as shown in (8), the moments of $\text{SIR}^{-1}$ are functions of $\lambda_B h_B^2$. Considering the height of the BS, the results are different from the analysis in [5]. Conclusions in [5] and [14] claim that with the increase of the density of BSs, the increase in signal power is exactly counterbalanced by the increase in interference power. It follows that the system performance including the cell coverage is independent of the density of BSs, which is referred as *density-invariance* [14].

The first two moments of the $\text{SIR}^{-1}$ can be calculated as

$$\begin{cases} m_1(\text{SIR}^{-1}) = \dfrac{2\Gamma\left(2, \pi\lambda_B h_B^2\right)}{\beta - 2} e^{\xi^2\sigma_\rho^2} \exp\left(\pi\lambda_B h_B^2\right) \\ m_2(\text{SIR}^{-1}) = \dfrac{\Gamma\left(2, \pi\lambda_B h_B^2\right)}{\beta - 1} e^{4\xi^2\sigma_\rho^2} \exp\left(\pi\lambda_B h_B^2\right) \\ \qquad\qquad + \dfrac{4\Gamma\left(3, \pi\lambda_B h_B^2\right)}{(\beta - 2)^2} e^{3\xi^2\sigma_\rho^2} \exp\left(\pi\lambda_B h_B^2\right). \end{cases}$$

### B. Analysis of SINR

As shown in (6), the reciprocal of SINR is expressed as the sum of the reciprocal of SNR and SIR,

$$(\text{SINR}^{-1})^n = (\text{SNR}^{-1} + \text{SIR}^{-1})^n. \tag{10}$$

Then the $n$th moment of $\text{SINR}^{-1}$ can be obtained based on the following lemmas.

*Lemma 2:* The $n$th moment of the $\text{SNR}^{-1}$ is expressed as

$$m_n(\text{SNR}^{-1}) = \frac{\sigma_N^{2n} A^{-n}}{P_t^n G_B^n} \exp\left(\pi\lambda_B h_B^2\right) (\lambda_B \pi)^{-\frac{n\beta}{2}} \times \Gamma\left(\frac{n\beta}{2} + 1, \pi\lambda_B h_B^2\right) \exp\left(\frac{n^2\xi^2\sigma^2}{2}\right).$$

*Proof:* The proof proceeds in a similar manner to Lemma 1 and so is omitted here. ■

*Lemma 3:* The $n$th moment of $\text{SINR}^{-1}$ can be expressed as shown in (11), at the bottom of the page, where $\binom{n}{i} = \frac{n!}{i!(n-i)!}$ represents the binomial coefficient.

*Proof:* The proof proceeds in a similar manner to Lemma 1 and so is omitted here. ■

## IV. System Performance

In this section, the system performance based on the approximate distribution of $\text{SINR}^{-1}$ is presented. Due to the difficulty in obtaining the distribution of the sum of log-normal random variables, the explicit expression for the distribution of SINR cannot be obtained. In this subsection, the log-Pearson type III (LP-III) distribution is adopted for the approximation of the distribution of $\text{SINR}^{-1}$ based on the moments of $\text{SINR}^{-1}$ as shown in (11). The LP-III distribution is

$$f_Z(z; \alpha, \beta, \delta) = \frac{(\ln z + \delta)^{\alpha-1}}{\beta^\alpha \Gamma(\alpha) z} \exp\left(\frac{\ln z - \delta}{\beta}\right), \quad 0 < z < e^\delta.$$

Based on the moment matching method, the parameters for the LP-III distribution are calculated as,

$$\begin{cases} (1 + \xi\beta)^{-\alpha} \exp(\xi\delta) = \mu_1 \\ (1 + 2\xi\beta)^{-\alpha} \exp(2\xi\delta) = \mu_2 \\ (1 + 3\xi\beta)^{-\alpha} \exp(3\xi\delta) = \mu_3, \end{cases} \tag{12}$$

where $\mu_n = m_n\left(\text{SINR}^{-1}\right), n = 1, 2, 3$ represent the $n$th moment of $\text{SINR}^{-1}$, respectively. Then the parameters for the LP-III distribution are calculated as,

$$\begin{cases} \beta = \left\{ x | \dfrac{(1+3x)^D}{1+2x} = (1+x)^{3D-2}, D = \dfrac{2\ln\mu_1 - \ln\mu_2}{3\ln\mu_1 - \ln\mu_3} \right\} \\ \alpha = \dfrac{2\ln\mu_1 - \ln\mu_2}{\ln(1+2\beta) - 2\ln(1+\beta)} \\ \delta = \ln\mu_1 + \alpha\ln(1+\beta). \end{cases}$$

The cell coverage is defined as the probability that SINR is larger than the threshold $T$, i.e., $P_c(T) = P(\text{SINR} > T) = P\left(\text{SINR}^{-1} < T^{-1}\right)$. Based on the approximate LP-III distribution for $\text{SINR}^{-1}$, the cell coverage can be calculated as

$$P_c(T) = P(\text{SINR}^{-1} < T^{-1}) = \begin{cases} 1 - \dfrac{\gamma\left(\alpha, \frac{-\ln T + \delta}{\beta}\right)}{\Gamma(\alpha)}, & 0 \leqslant T < e^\delta \\ 0, & T \geqslant e^\delta \end{cases} \tag{13}$$

$$m_n(\text{SINR}^{-1}) = \sum_{i=0}^{n} \binom{n}{i} \left[ \begin{matrix} \sigma_N^{2n-2i} (P_t G_B)^{i-n} A^{i-n} e^{\frac{n^2\xi^2\sigma_\rho^2}{2} + \frac{\xi^2(n-i)^2\sigma^2\rho}{2} + \pi\lambda_B h_B^2} \\ \times \sum\nolimits_{\bigcup_{p=1}^{q} I_p = I^i} 2^q (\pi\lambda_B)^{-\frac{n-i}{2}\beta} \Gamma\left(\frac{n-i}{2}\beta + q + 1, \pi\lambda_B h_B^2\right) \prod\limits_{p=1}^{q} \frac{\exp(n_p^2\xi^2\sigma_\rho^2/2)}{n_p\beta - 2} \end{matrix} \right] \tag{11}$$

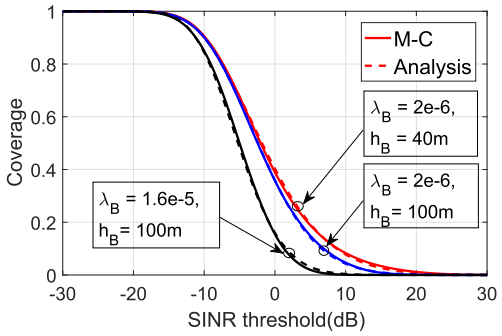


Fig. 2. Cell coverage vs $h_B$ and $\lambda_B$. Solid and dashed lines represent the Monte Carlo simulations and analysis, respectively.

TABLE I

PERFORMANCE COMPARISON OF THE LP-III AND THE LN APPROXIMATIONS IN TERMS OF CORRELATION COEFFICIENTS

| Parameter Setting | K-L Divergence | |
|---|---|---|
| | LP-III | LN |
| $\rho$ = 0 | 0.0027 | 0.0103 |
| $\rho$ = 0.5 | 0.0027 | 0.0294 |
| $\rho$ = 1 | 0.00388 | 0.1096 |

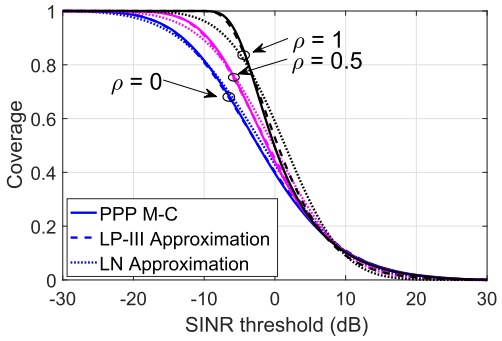


Fig. 3. Cell coverage for the different correlation coefficients of shadowing. Solid lines, dashed lines and dotted lines represent the cell coverage for the M-C simulations, LP-III approximations and log-normal (LN) approximations, respectively.

where $\gamma(s,x) = \int_0^x t^{s-1}e^{-t}dt$ is the lower incomplete Gamma function.

## V. NUMERICAL RESULTS

Numerical results of the cell coverage are illustrated in this section. The distance-dependent path loss at the reference distance and path loss exponent are $A = 10^{-7.2}$ and $\beta = 2.92$, respectively [15]. The standard deviation of shadowing is $\sigma = 6$ dB. The correlation coefficient for the shadowing is $\rho = 0.2$. The density of the BSs is $\lambda_B =$ 2e-6 BSs/m$^2$.

The cell coverage for the different height differences $h_B$s between BSs and UE and densities $\lambda_B$s of BSs are illustrated as shown in Fig. 2. The analytical results are close to the Monte Carlo (M-C) simulation results. As shown in Fig. 2, the cell coverage varies for the different $\lambda_B$s, which is different from the results in [5].

The cell coverage for the different correlation coefficients of shadowing are depicted in Fig. 3. The approximate LP-III distributions perfectly match with the distributions of Monte Carlo simulations, which show better accuracy compared with the log-normal approximations according to Table I. Moreover, as shown in Fig. 3, the cell coverage increases with the increase of correlation coefficient between the communication and interference links.

## VI. CONCLUSION

In the letter, the analysis for the system performance based on the PPP model is conducted. The impact for the height of BSs' antenna and the correlation coefficient of shadowing are studied. The closed-form expressions of moments for SIR$^{-1}$, SNR$^{-1}$ and SINR$^{-1}$ are presented. Analytical results show that $\lambda_B h_B^2$ is the underlying factor for the statistics of SIR. Numerical results indicate that the distribution of SINR$^{-1}$ can be well approximated by the log-Pearson type III distribution for various of system parameters. Moreover, cell coverage increases with the increase of the correlation coefficient between the communication and interference links.

## REFERENCES

[1] X. Yan, J. Xu, Y. Zhu, J. Wang, Y. Yang, and C.-X. Wang, "Downlink average rate and SINR distribution in cellular networks," *IEEE Trans. Commun.*, vol. 64, no. 2, pp. 847–862, Feb. 2016.

[2] B. Błaszczyszyn, M. K. Karray, and H. P. Keeler, "Using Poisson processes to model lattice cellular networks," in *Proc. IEEE INFOCOM*, Apr. 2013, pp. 773–781.

[3] H. Elsawy, E. Hossain, and M. Haenggi, "Stochastic geometry for modeling, analysis, and design of multi-tier and cognitive cellular wireless networks: A survey," *IEEE Commun. Surveys Tuts.*, vol. 15, no. 3, pp. 996–1019, 3rd Quart., 2013.

[4] H. ElSawy, A. Sultan-Salem, M. S. Alouini, and M. Z. Win, "Modeling and analysis of cellular networks using stochastic geometry: A tutorial," *IEEE Commun. Surveys Tuts.*, vol. 19, no. 1, pp. 167–203, 1st Quart., 2017.

[5] J. G. Andrews, F. Baccelli, and R. K. Ganti, "A tractable approach to coverage and rate in cellular networks," *IEEE Trans. Commun.*, vol. 59, no. 11, pp. 3122–3134, Nov. 2011.

[6] M. Ding and D. López-Pérez, "Performance impact of base station antenna heights in dense cellular networks," *IEEE Trans. Wireless Commun.*, vol. 16, no. 12, pp. 8147–8161, Dec. 2017.

[7] H. Wu *et al.*, "Content-aware cooperative transmission in HetNets with consideration of base station height," *IEEE Trans. Veh. Technol.*, to be published.

[8] *Spatial Channel Model for Multiple Input Multiple Output (MIMO) Simulations*, document TR 25.996, European Telecommunications Standards Institute, 2017.

[9] *Study on 3D Channel Model for LTE*, document TR36.873, V12.2.0, 3GPP, Mar. 2014.

[10] P. Agrawal and N. Patwari, "Correlated link shadow fading in multi-hop wireless networks," *IEEE Trans. Wireless Commun.*, vol. 8, no. 8, pp. 4024–4036, Aug. 2009.

[11] M. Di Renzo, A. Guidotti, and G. E. Corazza, "Average rate of downlink heterogeneous cellular networks over generalized fading channels: A stochastic geometry approach," *IEEE Trans. Commun.*, vol. 61, no. 7, pp. 3050–3071, Jul. 2013.

[12] J. Novak and P. Śniady, "What is a free cumulant," *Notices AMS*, vol. 58, no. 2, pp. 300–301, Feb. 2011.

[13] A. Rabbachin, T. Q. S. Quek, H. Shin, and M. Z. Win, "Cognitive network interference," *IEEE J. Sel. Areas Commun.*, vol. 29, no. 2, pp. 480–493, Feb. 2011.

[14] A. AlAmmouri, J. G. Andrews, and F. Baccelli, "SINR and throughput of dense cellular networks with stretched exponential path loss," *IEEE Trans. Wireless Commun.*, vol. 17, no. 2, pp. 1147–1160, Feb. 2018.

[15] M. R. Akdeniz *et al.*, "Millimeter wave channel modeling and cellular capacity evaluation," *IEEE J. Sel. Areas Commun.*, vol. 32, no. 6, pp. 1164–1179, Jun. 2014.